

Boundary Control of Inverters Using Second-Order Switching Surface

Kelvin K. S. Leung, Julian Y. C. Chiu and Henry S. H. Chung[†]

Department of Electronic Engineering
City University of Hong Kong
Tat Chee Avnue, Kowloon Tong, Kowloon, Hong Kong SAR, China
[†]Email: eeshc@cityu.edu.hk

Abstract – Concept of using a second-order switching surface in the boundary control of inverters is derived in this paper. The switching surface is formulated by estimating the state trajectory movement after a switching action. It results in a high state trajectory velocity along the switching surface. This phenomenon accelerates the trajectory moving towards the target operating point. Time-domain responses of the inverter with the proposed boundary control method under large-signal variations have been analyzed. The proposed control scheme has been successfully applied to a 100 W full-bridge inverter. Practical implementation of the system will be provided. Dynamic responses of the inverter supplying to different kinds of loads, including a resistive load, an inductive load, and a diode-capacitor rectifying circuit, have been studied. Experimental results show that the inverter output voltage can attain a low total harmonic distortion at different load conditions and fast response to a large-signal load disturbance and an output reference voltage change.

Index Terms - Boundary control, geometric control method, second-order switching surface, state trajectory control, inverters

I. INTRODUCTION

Nowadays, switch-mode inverters are widely used in power conditioning systems and ac motor drives. Their main function is to produce a sinusoidal ac output whose magnitude and frequency can be both controlled. Among various types of inverters, pulsewidth-modulated (PWM) inverter is the most popular one. Apart from high conversion efficiency, high-performance inverter requires high input stability and reliability, fast transient response, and low output impedance, total harmonic distortion (THD), and electromagnetic interference.

A typical PWM inverter system consists of a dc source, dc-ac inverter, and LC filter. In order to minimize the THD of the output voltage, many PWM modulation methods [1]-[3] have been used to regulate the fundamental component and eliminate the low-order harmonics. Moreover, many closed-loop control schemes have been proposed, in order to attain good dynamic response [4]-[6]. However, design of the feedback controller for those inverter systems is generally based on the small-signal linearized model. The inverter performance will deviate much from the expected profile if the inverter is subject to a large-signal disturbance.

Many research articles focus on studying the use of boundary control in inverter systems. Boundary control is a geometric based control approach suitable for switching converters [7, 8]. Its advantage lies in its generality of controlling converter operation without differentiating startup, transient, and steady

The work described in this paper was fully supported by a grant from the Research Grants Council of the Hong Kong Special Administrative Region, China (Project No. CityU 1319/04E).

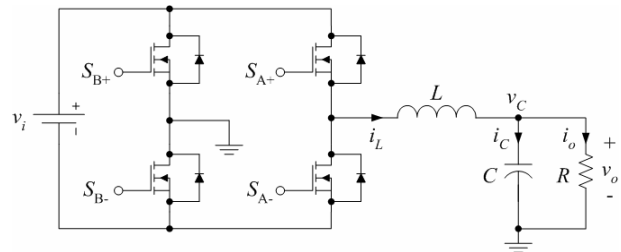


Fig. 1 Circuit schematic of typical full-bridge dc-ac inverter.

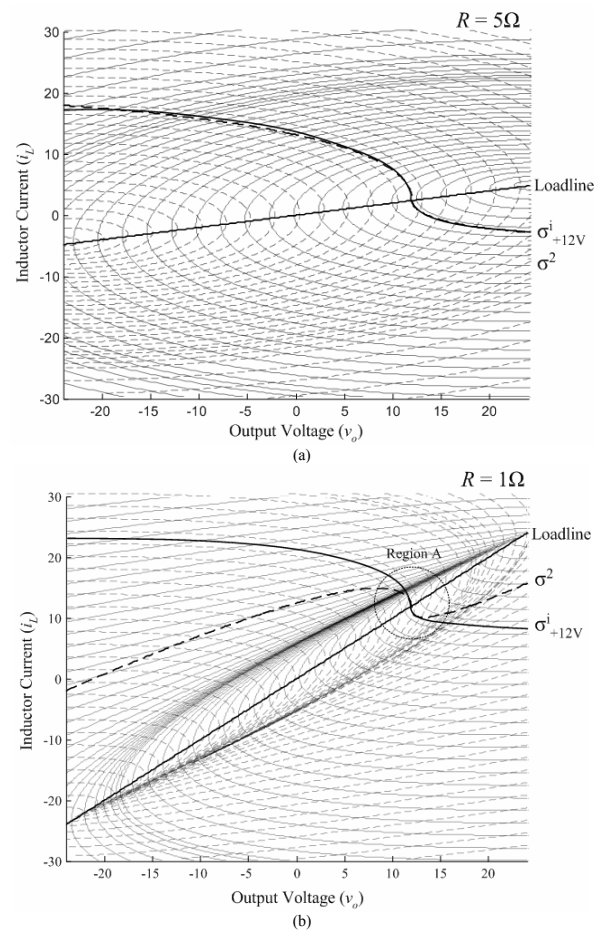


Fig. 2 Positive- and negative-state trajectories, loadline, σ^1 and σ^2 of the inverter. (a) $R = 5 \Omega$. (b) $R = 1 \Omega$.

state, so it is possible to deal with large-signal disturbances. The boundary control method is to drive the state trajectory of the inverter power stage onto a desired surface in the state space. Typical switching surface is a linear one (σ^1). Various σ^1 -derived boundary control methods, such as the sliding-mode control and hysteresis control, are widely studied for power converters [9]-[12]. All those methods provide good steady-state and large-signal response and stability, but the

transient dynamics is still non-optimal. Much research work extends the concepts, such as the adaptive hysteresis control in [13, 14], to enhance the dynamics.

Recently, boundary control using second-order switching surface (σ^2) has been proposed in [15] that the dynamic behaviors are better than σ^1 . By approximating the ideal switching surface with a second order function, σ^2 can achieve near-optimum large-signal response with simple implementation of the control circuit. In this paper, concept of σ^2 will be applied to control a dc-ac full-bridge inverter. The proposed control scheme has been successfully applied to a 100 W full-bridge inverter. Practical implementation of the system will be provided. Dynamic responses of the inverter supplying to different kinds of loads, including a resistive load, an inductive load, and a diode-capacitor rectifying circuit, have been studied. Experimental results show that the inverter output voltage can attain a low total harmonic distortion at different load conditions and fast response to a large-signal load disturbance and an output reference voltage change.

II. PRINCIPLE OF OPERATION

Fig. 1 shows a single-phase full-bridge dc-ac inverter. The inverter is supplied from a dc source v_i through a low-pass filter formed by L and C . The load is represented by a resistor R . Switches (S_{A+}, S_{B-}) are switched in anti-phase with (S_{A-}, S_{B+}). The system can be represented by the following state-space equations,

$$\dot{x} = A_0 x + B_0 u + (A_1 x + B_1 u) q_1 + (A_2 x + B_2 u) q_2 \quad (1)$$

where $x = [i_L \ v_C]$, $u = v_i$, A_n and B_n are constant matrix and q_i represents the state of the switches. (S_{A+}, S_{B-}) are on if $\{q_1, q_2\} = \{1, 0\}$, and (S_{A-}, S_{B+}) are on if $\{q_1, q_2\} = \{0, 1\}$. Matrices $A_0, B_0,$

A_1, B_1, A_2 and B_2 are defined as $A_0 = \begin{bmatrix} 0 & -1/L \\ 1/C & -1/RC \end{bmatrix}$,

$$B_0 = \begin{bmatrix} 0 \\ 0 \end{bmatrix}, \quad A_1 = \begin{bmatrix} 0 & 0 \\ 0 & 0 \end{bmatrix}, \quad B_1 = \begin{bmatrix} 1/L \\ 0 \end{bmatrix}, \quad A_2 = \begin{bmatrix} 0 & 0 \\ 0 & 0 \end{bmatrix},$$

$$B_2 = \begin{bmatrix} -1/L \\ 0 \end{bmatrix}.$$

A family of the state-space trajectories and the load line are shown in Fig. 2. Fig. 2(a) shows the characteristics when $R = 5 \ \Omega$. Fig. 2(b) shows the characteristics when $R = 1 \ \Omega$. The component values used in the analysis are tabulated in Table I. The trajectories consist of two main types - the positive-state trajectories and the negative-state trajectories. They are obtained by solving (1) with different initial conditions. The positive-state trajectory is obtained by setting $\{q_1, q_2\} = \{1, 0\}$, while the negative-state trajectory is obtained by setting $\{q_1, q_2\} = \{0, 1\}$. As discussed in [7], the tangential component of the state-trajectory velocity on the switching surface determines the rate at which successor points approach or recede from the target operating point. An ideal switching surface σ^i that gives optimum dynamics should be on the only trajectory passing through the target operating point. σ^i for target operating point at +12 V is shown in Fig. 2. For dc-ac application, the output voltage v_o is time varying and follow the reference signal. Therefore, the target operating point of σ^i is also time-dependent. Although σ^i can achieve steady-state operation for a step change in the output current or reference voltage in one on/off control, it is load-dependent and requires

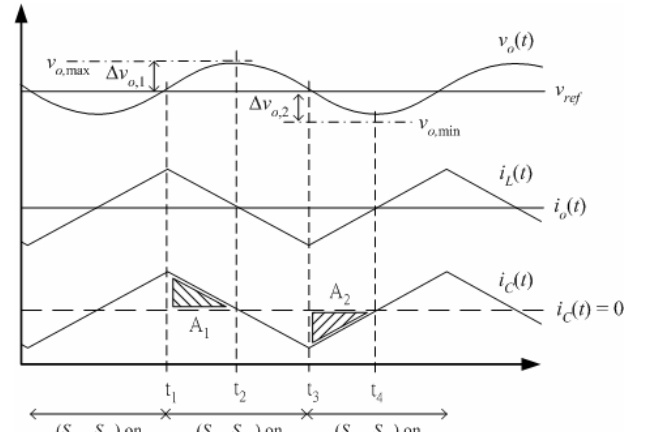


Fig. 3 Typical waveforms of v_o, i_L, i_o and i_C .

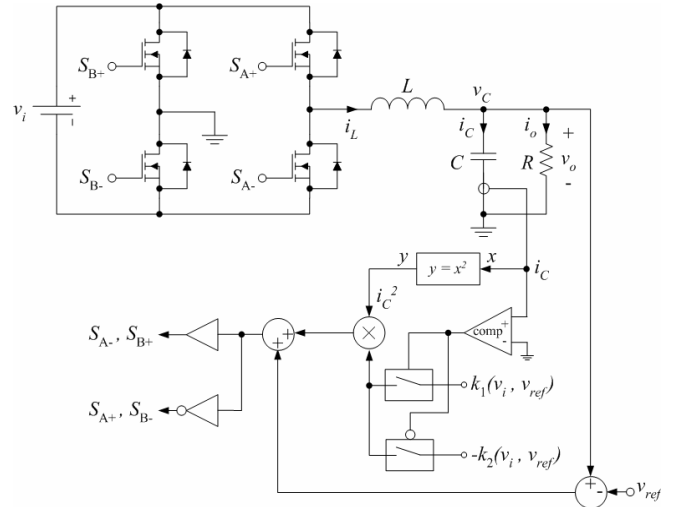


Fig. 4 Implementation of the controller.

sophisticated computation for solving the only positive- and negative-state trajectory that passes each of the target operating points in a time varying system.

A second-order surface σ^2 , which is close to the ideal surface around the operating point, is derived in the following. The concept is based on estimating the state trajectory after a hypothesized switching action. As the switching frequency of the switches is much higher than the signal frequency, the output current i_o is relatively constant over a switching cycle. The gate signals to the switches are determined by the following criteria.

A. Criteria for switching on (S_{A-}, S_{B+})

Fig. 3 shows the typical waveforms of v_o, i_L, i_o and i_C . (S_{A-}, S_{B+}) are originally off and are switched on at the hypothesized time instant t_1 , so that v_o equals $v_{o,max}$ at t_2 (at which $i_C = 0$). Thus,

$$i_C = C \frac{dv_C}{dt} = C \frac{dv_o}{dt} \quad (2)$$

$$-(v_i + v_o) = L \frac{di_L}{dt} \quad (3)$$

By using $i_L = i_C + i_o$ and assuming i_o to be constant,

$$\frac{di_C}{dt} = \frac{di_L}{dt} = -\frac{v_i + v_o}{L} \Rightarrow dt = -\frac{L}{v_i + v_o} di_C \quad (4)$$

Based on (2),

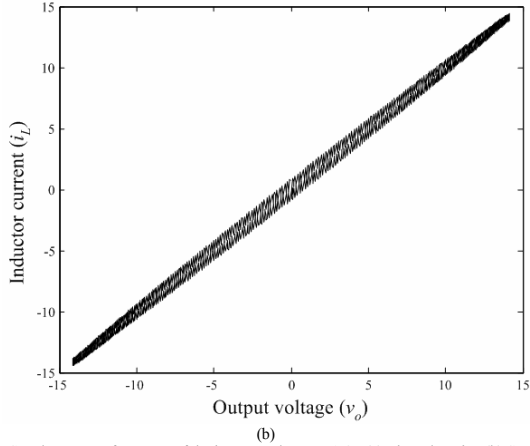
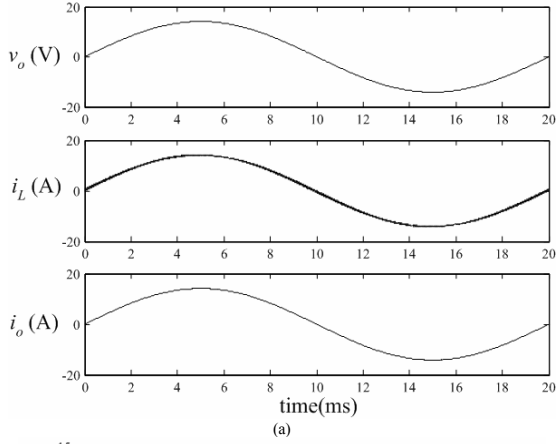


Fig. 5 Steady-state performance of the inverter when $R = 1 \Omega$. (a) Time-domain. (b) State-plane.

$$\Delta v_{o,1} = v_o(t_2) - v_o(t_1) = v_{o,\max} - v_o(t_1) = \frac{1}{C} \int_{t_1}^{t_2} i_C dt \quad (5)$$

By substituting (4) and $i_C(t_2) = 0$ into $\frac{1}{C} \int_{t_1}^{t_2} i_C dt$, eq. (5) can be expressed to ensure that v_o will not go above $v_{o,\max}$, (S_{A-} , S_{B+}) should be switched on when

$$v_o(t_1) \geq v_{o,\max} - \frac{L}{2C(v_i + v_o)} i_C^2(t_1) = v_{o,\max} - k_1(v_i, v_o) i_C^2(t_1) \quad (6)$$

and

$$i_C(t_1) > 0 \quad (7)$$

B. Criteria for switching on (S_{A+} , S_{B-})

As shown in Fig. 3, (S_{A+} , S_{B-}) are originally off and are switched on at the hypothesized time instant t_3 , so that v_o equals $v_{o,\min}$ at t_4 (at which $i_C = 0$). Thus,

$$i_C = C \frac{dv_C}{dt} = C \frac{dv_o}{dt} \quad (8)$$

$$v_i - v_o = L \frac{di_L}{dt} \quad (9)$$

By using $i_L = i_C + i_o$ and assuming i_o to be constant,

$$dt = \frac{L}{v_i - v_o} di_C \quad (10)$$

Based on (8),

$$\Delta v_{o,2} = v_o(t_4) - v_o(t_3) = v_{o,\min} - v_o(t_3) = \frac{1}{C} \int_{t_3}^{t_4} i_C dt \quad (11)$$

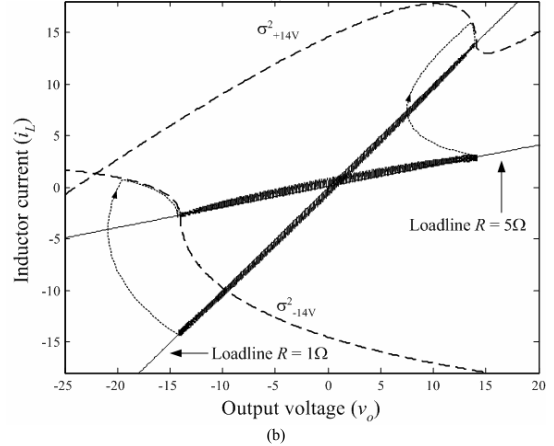
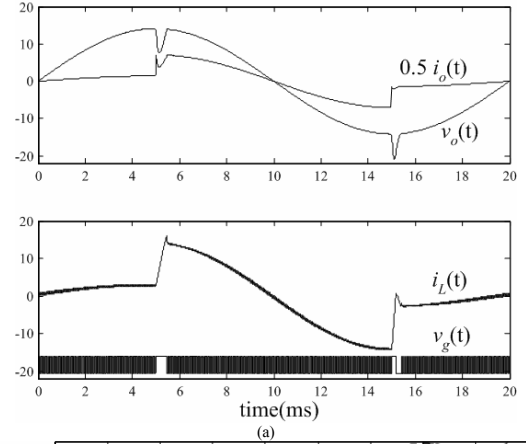


Fig. 6 dynamics performance of the inverter under load change from 5Ω to 1Ω and vice versa. (a) Time-domain. (b) State-plane.

By substituting (10) and $i_C(t_4) = 0$ into $\frac{1}{C} \int_{t_3}^{t_4} i_C dt$, eq. (11) can be expressed to ensure that v_o will not go below $v_{o,\min}$, (S_{A+} , S_{B-}) should be switched on when

$$v_o(t_3) \leq v_{o,\min} + \frac{L}{2C(v_i - v_o)} i_C^2(t_3) = v_{o,\min} + k_2(v_i, v_o) i_C^2(t_3) \quad (12)$$

and

$$i_C(t_3) < 0 \quad (13)$$

Based on (6), (7), (12), (13) and $v_{o,\min} = v_{o,\max} = v_{ref}$, the following σ^2 can be concluded,

$$\sigma^2(i_C, v_o) = \begin{cases} k_1 i_C^2 + (v_o - v_{ref}), & i_C > 0 \\ -k_2 i_C^2 + (v_o - v_{ref}), & i_C < 0 \end{cases} \quad (14)$$

The equation can further be written into a single expression of $\sigma^2(i_C, v_o) = c_2 i_C^2 + (v_o - v_{ref})$ (15)

where $c_2 = \frac{k_1}{2}(1 + \text{sgn}(i_C)) - \frac{k_2}{2}(1 - \text{sgn}(i_C))$.

σ^2 consists of a second-order term and is close to σ^1 near the operating point. However, discrepancies occur, when the state is far from the operating point because of the approximations in (4) and (10). Fig. 2 shows that the discrepancy increases between σ^1 and σ^2 when R decreases. However, near the target operating point (“Region A”), both σ^1 and σ^2 are still approximately equal. A phenomenon can be observed from Fig. 2(b), for any initial states below σ^2 . The positive-state trajectory finally enters “Region A”, where σ^2 maintains the ideal switching surface property. Practically, the discrepancy does not affect the inverter performance.

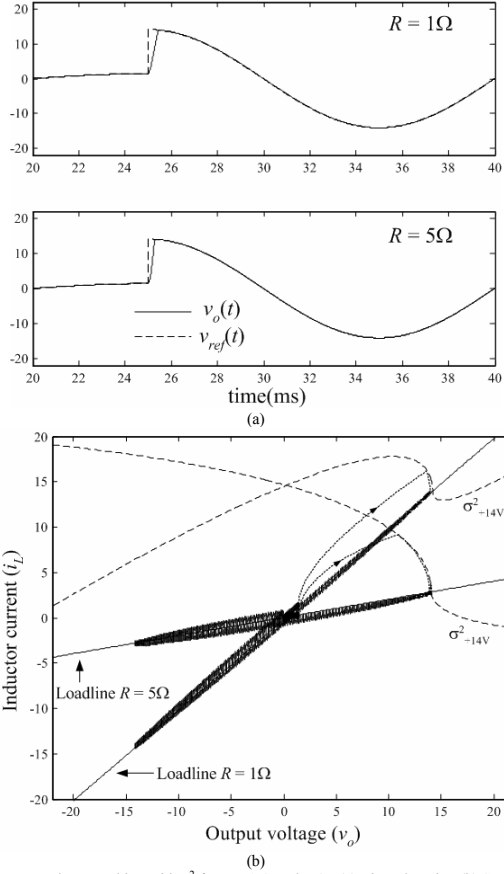


Fig. 7 Output voltage tracking with σ^2 for $R = 1 \Omega$ and 5Ω . (a) Time-domain. (b) State-plane.

The control circuit can be implemented by using simple analog devices. Multipliers are required to compute the function of k_1 , k_2 , and i_C^2 , the remaining parts can be handled by using a simple logic circuitry. Fig. 4 shows the block diagram of the controller.

III. LARGE-SIGNAL STABILITY

Points along $\sigma = 0$ can be classified into refractive, reflective, and rejective modes. The dynamics of the system will be exhibited differently in these regions. For σ^2 , the transition boundary is obtained by differentiating (15) so that

$$\left. \frac{di_L}{dv_o} \right|_{on,off} = \frac{1}{R} + \frac{1}{2} \frac{i_L - \frac{v_o}{R}}{v_o - v_{ref}} \quad (16)$$

The expression at the left-hand side can be derived by using the state equations in (1). Based on (16), the transition boundary with (S_{A+}, S_{B-}) on is

$$\frac{C}{L} \left(\frac{v_i - v_o}{i_L - \frac{v_o}{R}} \right) = \frac{1}{R} + \frac{1}{2} \frac{i_L - \frac{v_o}{R}}{v_o - v_{ref}} \quad (17)$$

And the transition boundary with (S_{A-}, S_{B+}) on is

$$-\frac{C}{L} \left(\frac{v_i + v_o}{i_L - \frac{v_o}{R}} \right) = \frac{1}{R} + \frac{1}{2} \frac{i_L - \frac{v_o}{R}}{v_o - v_{ref}} \quad (18)$$

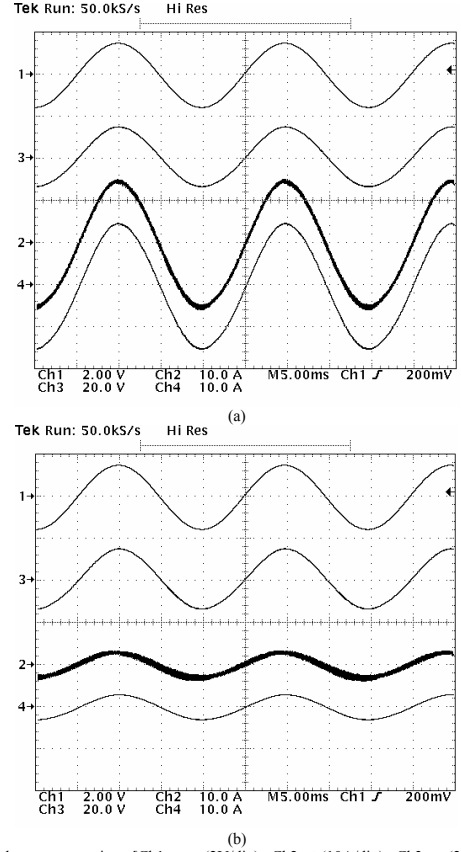


Fig. 8 Steady-state operation. [Ch1: v_{ref} (2V/div), Ch2: i_L (10A/div), Ch3: v_o (20V/div), Ch4: i_o (10A/div)]. (a) $R = 1 \Omega$ (full load). (b) $R = 5 \Omega$.

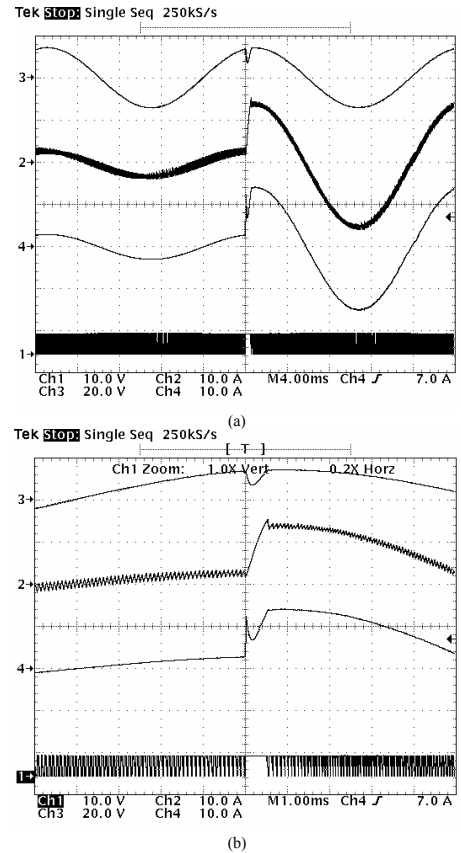


Fig. 9 Transient response of the full-bridge inverter when R change from 5Ω to 1Ω . [Ch1: v_i (10 V/div), Ch2: i_L (10 A/div), Ch3: v_o (20 V/div), Ch4: i_o (10 A/div)]. (a) Timebase = 4ms. (b) Timebase = 1ms.

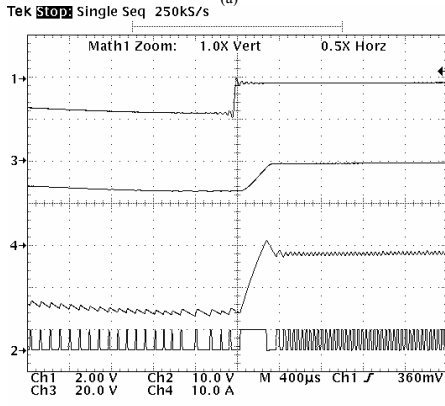
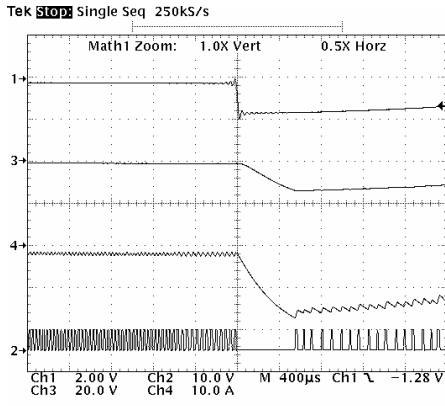


Fig. 10 Output voltage tracking when $R = 1 \Omega$. [Ch1: v_{ref} (2 V/div), Ch2: v_g (10 V/div), Ch3: v_o (20 V/div), Ch4: i_L (10 A/div)]. (a) v_{ref} increases from 1 V_{rms} to 10 V_{rms}. (b) v_{ref} decreases from 10 V_{rms} to 1 V_{rms}.

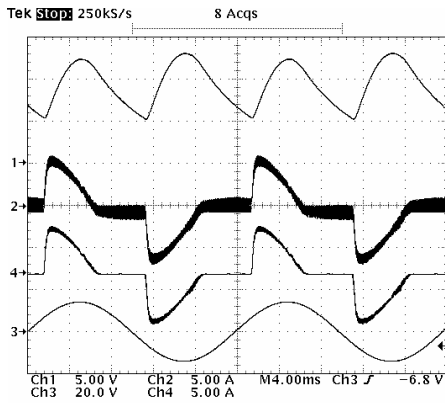


Fig. 11 Steady-state output for a full-wave rectifier load. [Ch1: $v_{o,rectified}$ (5 V/div), Ch2: i_L (5 A/div), Ch3: v_o (20 V/div), Ch4: i_o (5 A/div)].

IV. SIMULATION VERIFICATIONS

An inverter with the component values tabulated in Table I is studied. Fig. 5 shows the steady-state performance of the inverter operated at $R = 1 \Omega$ and $v_{o,rms} = 10 \text{ V}_{rms}$. Fig. 6 shows the dynamic responses (the time-domain waveforms in Fig. 6(a) and the phase plane in Fig. 6(b)) of the inverter under a load change from 5Ω to 1Ω and vice versa. σ^2 determines the switching actions of the switches when the converter is subject to a large signal disturbance. In fig. 6(b), just before the load change from 1Ω to 5Ω , the output voltage is approximately equal to 14 V ($i_o = 14 \text{ A}$). When the load change to 5Ω , $[i_L \ v_o]$ below σ^2 and the movement of $[i_L \ v_o]$ will follow the positive-state trajectory until it touch the switching surface. σ^2 is nearly the same as the ideal switching surface when the final states of $[i_L \ v_o]$ is near the target operating point. Therefore, the output can revert back to the ac profile in two switching action.

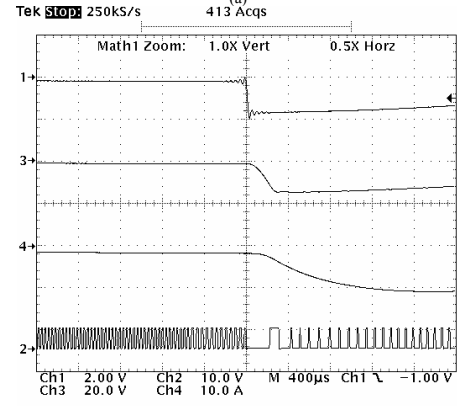
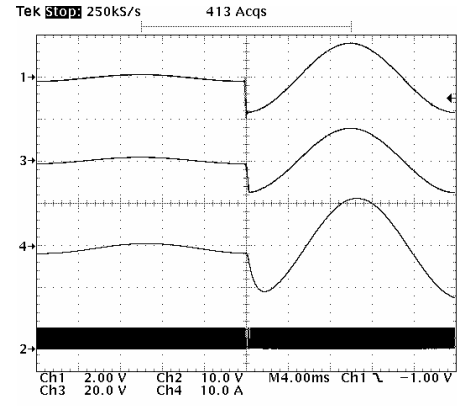


Fig. 12 Output voltage tracking with inductive load. [Ch1: v_{ref} (2 V/div), Ch2: v_g (10 V/div), Ch3: v_o (20 V/div), Ch4: i_o (10 A/div)]. (a) Timebase = 4ms. (b) Timebase = 400μs.

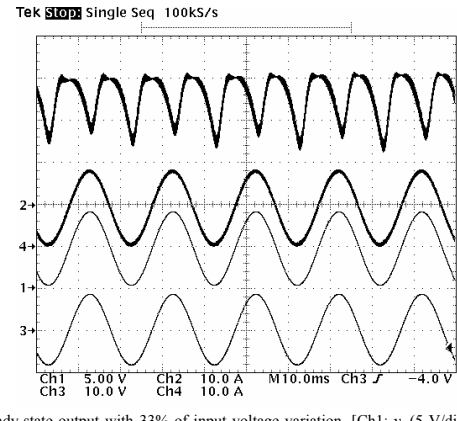


Fig. 13 Steady-state output with 33% of input voltage variation. [Ch1: v_i (5 V/div), Ch2: i_L (10 V/div), Ch3: v_o (10 V/div), Ch4: i_o (10 A/div)].

Fig. 7 shows the simulated time-domain waveforms and state trajectories of the converter when v_{ref} is suddenly changed.

V. EXPERIMENTAL VERIFICATIONS

A 100 W full bridge inverter has been built to verify the theoretical prediction and simulation results. The component values of the experimental prototype are tabulated in Table I. Fig. 8 shows the steady state operation when $R = 1 \Omega$ (full load) and $R = 5 \Omega$. The output voltage is regulated at 10 V_{rms} . Fig. 9 shows the transient response when R is changed from 5Ω to 1Ω . The output voltage can revert to the ac reference within two switching actions. Fig. 10 shows the output voltage tracking performance when $R = 1 \Omega$, a 50 Hz ac reference, dynamic change from 10 V_{rms} to 1 V_{rms} is used to demonstrate the voltage tracking ability of the controller. Again, the output voltage can

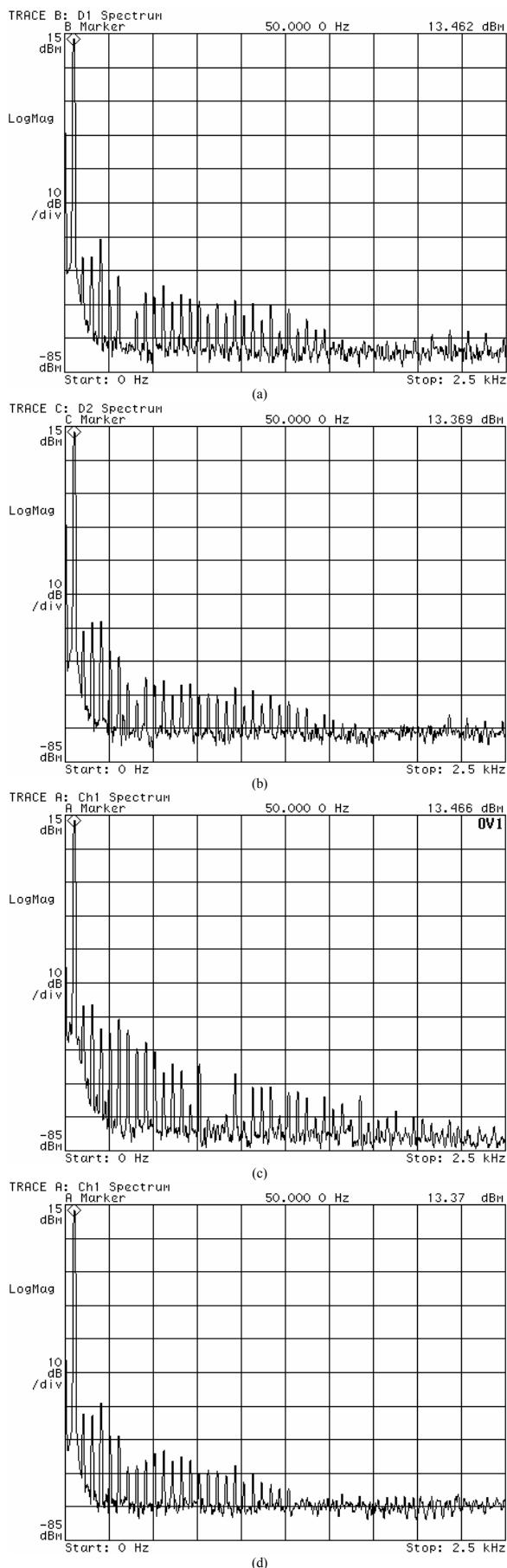


Fig. 14 Harmonic spectra of the output voltage v_o for different loading condition. (a) Resistive load for $R = 5 \Omega$. (b) Resistive load for $R = 1 \Omega$. (c) Full wave rectified load for $P_o = 36 \text{ W}$. (d) Inductive load for $L = 1 \text{ mH}$, $R = 1 \Omega$.

obtain near optimal response for increasing or decreasing of voltage reference.

In practical application, a full-wave rectifier may be connected to the output of the full-bridge inverter for providing a rectified dc. Fig. 11 shows the steady-state output for a full-wave rectifier load with $i_{o,rms} = 2.76 \text{ A}$ and $v_{o,rectified} = 9.3 \text{ V}$. Another practical loading condition is the inductive loading. Fig. 12 shows the output voltage with an inductive load, which is formed by connecting a 1 mH inductor in series with a 1Ω resistor. A phase shift of 17.4° (0.97 ms) between v_o and i_o is observed.

Finally, the DC input voltage source is replaced by a diode-capacitor rectifying circuit with input capacitance equal to $2000 \mu\text{F}$ in order to show the inverter performance with input voltage variation. Fig. 13 shows the response of the inverter operating at 36 W , the controller is insensitive with the input voltage and even 33% (8.4 V_{p-p}) change in input voltage does not affect the output waveform. Fig. 14 shows the harmonic spectra of the output voltage v_o for different loading condition. Table II shows the total harmonic distortions (THDs) of the output voltage with four loads in Fig. 14. They are all below 0.3%.

TABLE I
COMPONENT VALUES OF THE FULL BRIDGE INVERTER

| Parameter | Value |
|-----------|-------------------|
| v_i | 24 V |
| L | 500 μH |
| C | 100 μF |
| R | 1 Ω |

TABLE II
TOTAL HARMONIC DISTORTIONS (THDs) OF THE OUTPUT VOLTAGE

| $v_o = 10 \text{ V}_{rms}$ Noise Level = -80 dB Signal Freq = 50 Hz THD calculation Freq Band: 0Hz to 2.5kHz (>43 orders) | |
|--|-------------|
| Loading Condition | THD + N% |
| Resistive load for $R = 5 \Omega$. | 0.178046905 |
| Resistive load for $R = 1 \Omega$. | 0.275200479 |
| Full wave rectified load for $P_o = 36 \text{ W}$. | 0.306318266 |
| Inductive load for $L = 1 \text{ mH}$, $R = 1 \Omega$. | 0.206875159 |

VI. CONCLUSIONS

A second-order switching surface for boundary control of DC-AC inverter is proposed in this paper. The control method is simple and does not require any complicated calculation of the system transfer function or control loop compensation. The output voltage can obtain near-optimal response when it is subject to large-signal disturbances or input voltage variation. The control methods have been studied experimentally with a 100 W inverter prototype and provide good agreement with theoretical prediction.

REFERENCES

- [1] K. Taniguchi, Y. Ogino and H. Irie, "PWM Technique for Power MOSFET Inverter," *IEEE Trans. on Power Electronics*, vol. 3, no. 3, pp. 328-334, July 1988.
- [2] J. Holtz, "Pulsewidth Modulation for Electronic Power Conversion," *Proc. IEEE*, vol. 82, pp.1194-1214, Aug. 1994.
- [3] J. W. Kolar, H. Ertl, F. C. Zach, "Influence of the Modulation Method on the Conduction and Switching Losses of a PWM Converter System," *IEEE Trans. on Industry Applications*, vol. 27, no. 6, pp. 1063-1075, Nov.-Dec. 1991.

- [4] N. Hur, J. Jung, K. Nam, "A Fast Dynamic DC-Link Power-Balancing Scheme for a PWM Converter-Inverter System," *IEEE Trans. on Industrial Electronics*, vol. 48, no. 4, pp. 794-803, August 2001.
- [5] J. C. Liao, S. N. Yeh, "A Novel Instantaneous Power Control Strategy and Analytic Model for Integrated Rectifier / Inverter Systems," *IEEE Trans. on Power Electronics*, vol. 15, no. 6, pp. 996-1006, Nov. 2000
- [6] J. Holtz, B. Beyer, "Optimal Synchronous Pulsewidth Modulation with a Trajectory-Tracking Scheme for High-Dynamic Performance," *IEEE Trans. on Industry Applications*, vol. 29, no. 6, pp. 1098-1105, Nov.-Dec. 1993
- [7] R. Munzert and P. T. Krein, "Issues in boundary control," in *Record, IEEE Power Electronics Specialists Conf.*, 1996, pp. 810-816.
- [8] R. M. Bass, and P. T. Krein, "Switching boundary geometry and the control of single-phase inverters," in *Record, IEEE Industry Applications Society Annual Meeting*, 1989, pp. 1052-1056.
- [9] M. Greuel, R. Muysshondt and P. T. Krein, "Design Approaches to Boundary Controllers" in *Record, IEEE Power Electronics Specialists Conf.*, 1997, pp. 672-678.
- [10] D. Biel, E. Fossas, F. Guinjoan, E. Alarcon and A. Poveda, "Application of Sliding-Mode Control to the Design of a Buck-Based Sinusoidal Generator," *IEEE Trans. on Power Electronics*, vol. 48, no. 3, pp. 563-571, June 2001.
- [11] R. R. Ramos, D. Biel, E. Fossas and F. Guinjoan, "A Fixed-Frequency Quasi-Sliding Control Algorithm: Application to Power Inverters Design by Means of FPGA Implementation," *IEEE Trans. on Power Electronics*, vol. 18, no. 1, pp. 344-355, January 2003.
- [12] W. M. P. Filho, A. J. Perin, "An Approach of the Variable Structure Analysis for Power Electronics Applications," in *Record, IEEE Industry Applications Society Annual Meeting*, 1997, pp. 844-851
- [13] V. M. Nguyen and C. Q. Lee, "Tracking control of buck converter using sliding-mode with adaptive hysteresis," in *Record, IEEE Power Electronics Specialists Conf.*, 1995, pp. 1086-1093.
- [14] S. C. Tan, Y. M. Lai, M. K. H. Cheung, and C. K. Tse, "An Adaptive Sliding Mode Controller for Buck Converter in Continuous Conduction Mode," in *Proc. IEEE Applied Power Electronics Conf. Expo*, Feb. 2004, pp. 1395-1400
- [15] K. K. S. Leung and H. S. H. Chung, "Derivation of a Second-Order Switching Surface in the Boundary Control of Buck Converters," *IEEE Power Electronics Letter*, vol. 2, no. 2, pp. 63-67, June 2004.